THESIS FOR THE DEGREE OF LICENTIATE OF ENGINEERING

Force-based Perception and Control Strategies for Human-Robot Shared Object Manipulation

Ramin Jaberzadeh Ansari

CHALMERS
UNIVERSITY OF TECHNOLOGY

Department of Electrical Engineering
Chalmers University of Technology
Göteborg, Sweden, 2019

Force-based Perception and Control Strategies for Human-Robot Shared Object Manipulation

Ramin Jaberzadeh Ansari

Department of Electrical Engineering
Chalmers University of Technology
SE-412 96 Göteborg, Sweden
Telephone: +46 (0)31 772 1000
www.chalmers.se

This thesis has been prepared using LaTeX.

Printed by Chalmers Reproservice
Göteborg, Sweden, November 2019

To my family

Abstract

Physical Human-Robot Interaction (PHRI) is essential for the future integration of robots in human-centered environments. In these settings, robots are expected to share the same workspace, interact physically, and collaborate with humans to achieve a common task. One of the primary tasks that require human-robot collaboration is object manipulation. The main challenges that need to be addressed to achieve a seamless cooperative object manipulation are related to uncertainties in human trajectory, grasp position, and intention. The object's motion trajectory intended by the human is not always defined for the robot and the human may grasp any part of the object depending on the desired trajectory. In addition, the state-of-the-art object-manipulation control schemes suffer from the translation/rotation problem, where the human cannot move the object in all degrees of freedom, independently, and thus, needs to exert extra effort to accomplish the task.

To address the challenges, first, we propose an estimation method for identifying the human grasp position. We extend the conventional contact point estimation method by formulating a new identification model with the human applied torque as an unknown parameter and employing empirical conditions to estimate the human grasp position. The proposed method is compared with a conventional contact point estimation using the experimental data collected for various collaboration scenarios. Second, given the human grasp position, a control strategy is suggested to transport the object in all degrees of freedom, independently. We employ the concept of "the instantaneous center of zero velocity" to reduce the human effort by minimizing the exerted human force. The stability of the interaction is evaluated using a passivity-based analysis of the closed-loop system, including the object and the robotic manipulator. The performance of the proposed control scheme is validated through simulation of scenarios containing rotations and translations of the object.

Our study indicates that the exerted torque of the human has a significant effect on the human grasp position estimation. Besides, the knowledge of the human grasp position can be used in the control scheme design to avoid the translation/rotation problem and reduce the human effort.

Keywords: physical human-robot collaboration, kinesthetic perception, human-robot interaction control, system identification

Acknowledgments

First and foremost, I would like to thank my supervisors, Assistant Professor Yiannis Karayiannidis and Professor Jonas Sjöberg, for giving me the opportunity to work on an exciting and challenging topic. Thanks for all the fruitful discussions and continuous encouragement. Your guidance has been a valuable input for this thesis.

I also would like to thank my colleagues in the Systems and Control group for a friendly work environment. Specifically, I would like to show my appreciation to Giuseppe and Albin for providing valuable feedback on this work. I am also thankful to everyone at the Electrical Engineering Department for making Chalmers an excellent workplace for me. Besides, I would like to acknowledge my colleagues at Volvo Trucks, especially Per-Lage Götvall, for inspiring me in the early stages of this research.

In addition, I would like to thank all my friends who have made my stay here in Sweden memorable.

Finally, my deep and sincere gratitude to my family, especially my parents, for their continuous and unparalleled love, help, and support. In particular, I would like to express my gratitude towards my wife, Samar, for her endless support and love.

Ramin Jaberzadeh Ansari
Göteborg, Sweden, November 2019

List of Publications

This thesis is based on the following publications:

[A] **R. Jaberzadeh Ansari**, G. Giordano, J. Sjöberg, Y. Karayiannidis, "Human Grasp Position Estimation for Human-Robot Cooperative Object Manipulation," Submitted to *Robotics and Autonomous Systems Journal*.

[B] **R. Jaberzadeh Ansari**, Y. Karayiannidis, "Reducing the Human Effort for Human-Robot Cooperative Object Manipulation via Control Design," *20th World Congress of the International Federation of Automatic Control (IFAC)*, Toulouse, France, 2017.

Other related publications of the Author not included in this thesis:

- **R. Jaberzadeh Ansari**, Y. Karayiannidis, J. Sjöberg, "Physical Human-Robot Interaction through a Jointly-Held Object based on Kinesthetic Perception," *27th IEEE International Symposium on Robot and Human Interactive Communication (RO-MAN)*, Nanjing, China, 2018.
  Awarded Nanjing City Prize in IEEE RO-MAN 2018.

Acronyms

Cobot:	Collaborative Robot
DoF:	Degrees of Freedom
F/T:	Force/Torque
HRC:	Human-Robot Collaboration
IO:	Input-Output
LSM:	Least-Squares Method
MD:	Maximum Deviation
PHRI:	Physical Human-Robot Interaction
PHRC:	Physical Human-Robot Collaboration
RLS:	Recursive Least Squares
SMEs:	Small and Medium-sized Enterprises

Contents

Part I

Overview

CHAPTER 1

Introduction

Robotics has revolutionized various industries over the last decades by offering high speed, precision, and endurance with respect to human workers. However, robots do not have the level of human intelligence and adaptability to new environments. To combine the best qualities of humans and robots, Human-Robot Collaboration (HRC) has received attention from several research groups in industry and academia. Some examples of HRC applications include assistance in production [1], emergency rescue operation [2], space exploration [3], and social service [4]. HRC requires communication between the human and the robot to achieve a common goal. The prominent communication channels in HRC are vision and haptics [5], [6]. In particular, haptic feedback is tightly connected to Physical Human-Robot Collaboration (PHRC) that involves Physical Human-Robot Interaction (PHRI).

PHRC applications have been restricted due to the safety issues related to traditional industrial robots. In this regard, cobots (collaborative robots) are developed for operating in the vicinity of humans and assisting them in accomplishing tasks. Unlike traditional industrial robots, cobots are not confined to cages and are safer for physical interaction with humans (Fig. 1.1). Human safety is improved by introducing new regulations for safety-related

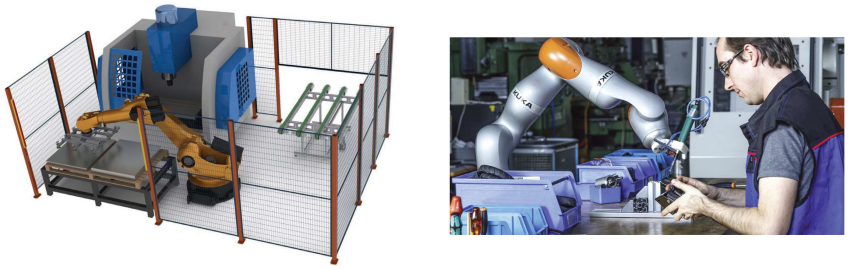

Figure 1.1: Non-collaborative robots vs collaborative robots [8]

functions and features [7].

The main motivations of employing cobots are better accuracy, improved efficiency in terms of time and energy, positive economic impact, and persistent help for humans. Additionally, they are expected to achieve higher levels of cooperation and communication with humans in the near future [9], including social interactions [10].

According to the available statistical data [11], the current market for cobots is worth about 710 million USD and expected to grow to 12303 million USD by 2025, corresponding to 30% of the total robots' market. Although the automotive and electronic industries are the largest consumers of the cobots, the increase is also attributed to the interest of Small and Medium-sized Enterprises (SMEs) to employ cobots for performing tasks traditionally allocated to human operators [12]. Cobots are appealing solutions for further development of SMEs, given their simple installation, flexible deployment, and user-friendly interfaces.

Cobots have the potential to perform many operations autonomously or collaboratively with humans. Some essential operations are material handling, assembly, and pick & place [12]. These operations require various tasks, such as object manipulation, tool pick-and-place, etc. In this thesis, we focus on human-robot cooperative object manipulation using cobots. An example of such a task is shown in Fig. 1.2, where a cobot assists a human to transport an object. The human decides about the target location of the object, and the cobot provides the human with the support by carrying the load of the object. The cobot measures the interaction wrench, i.e., force and torque, using either the torque sensors at its joints or the dedicated force/torque sensor installed at its end-effector. The interaction wrench can be employed to perceive the

environment and also create a control command for the cobot.

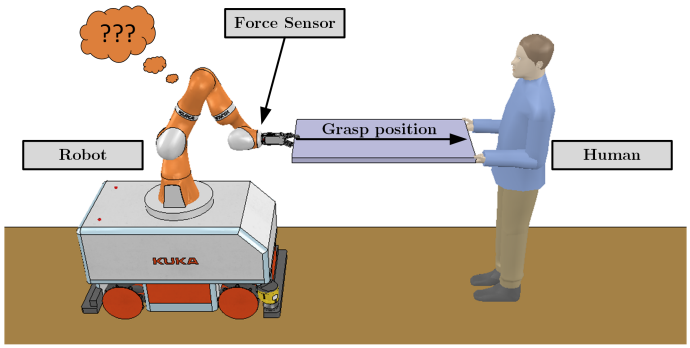

Figure 1.2: PHRC scenario of shared object manipulation

This thesis studies control and estimation algorithms to facilitate physical human-robot interaction through a jointly grasped object. In particular, we address the following problems:

- Human grasp localization using force/torque measurements: The human may grasp any part of the object to have control over the motion by applying forces and torques on the object. In case of pure human force, the problem will be simplified to a contact point estimation/localization ([13], [14]). However, the estimation becomes a difficult task when the human is simultaneously exerting force and torque [14].

- Transparency of human haptic commands: In case of physical interaction, the intention is reflected through the haptic commands, i.e., the interaction forces. If there is no object between the human and the cobot, the human may apply wrench along the intended direction of the motion. However, the object between the cobot and the human modifies the kinesthetic mapping of the human forces and distorts the human intention. Consequently, the resulting motion does not correspond to the human intention.

1.1 Thesis outline and contributions

A shared object manipulation scenario is considered in this thesis, as shown in Fig. 1.2. First, we examine the effect of the human applied torque on the grasp position estimation, and we propose a strategy to evaluate the quality of the estimates. The proposed method employs a least-squares method and accepts or rejects the result based on the defined conditions. The performance of the method is compared with conventional contact point estimation using the experimental data from a robotic setup that includes a UR10 collaborative robot and force/torque sensors for collecting wrench data. The experimental data are collected during the collaboration scenarios that the human applies both force and torque on the object. Second, we propose a control method for the object manipulation task that correlates the motion of the object with the human intention by compensating for the distance between the robot and the human. The proposed control method also reduces the human effort during the operation.

The thesis consists of two main parts. Part I is a summary of the research area, concepts, and proposed methods. In this regard, Chapter 2 provides background information on the object, human arm, and robot models and introduces a parameter estimation method that is used in the thesis. Chapter 3 introduces the human grasp position estimation problem and the proposed estimation scheme. Chapter 4 presents the interaction dynamics and common control strategies for object transportation tasks. Chapter 5 provides a summary of the appended papers, the concluding remarks, and the future works. The papers are appended in Part II.

CHAPTER 2

Preliminaries

This chapter provides an overview of the methods used in the thesis. Section 2.1 describes the 6 Degrees of Freedom (DoF) dynamics of an object. Section 2.2 introduces a linear dynamic model considered for a human arm. The general dynamics of robot manipulators and an overview of interaction control schemes are presented in Section 2.3. Section 2.4 gives a brief overview of the general form of an unconstrained least-squares method for parameter identification accompanied by the derivation of the recursive form.

2.1 Object dynamics

The free-body diagram of an object is shown in Fig. 2.1. The position and orientation of a rigid object is described using 6 independent parameters denoted by $\boldsymbol{x}_o = [\boldsymbol{p}_o^T, \boldsymbol{\phi}_o^T]^T \in \mathbb{R}^6$, where the vector $\boldsymbol{p}_o \in \mathbb{R}^3$ represents the position of the object's center of mass and the vector $\boldsymbol{\phi}_o \in \mathbb{R}^3$ denotes the orientation of the fixed body frame located at the center of mass. The vector $\boldsymbol{v}_o = [\dot{\boldsymbol{p}}_o^T, \boldsymbol{\omega}_o^T]^T \in \mathbb{R}^6$ represents linear and angular velocities, where $\boldsymbol{\omega}_o = \boldsymbol{T}(\boldsymbol{\phi}_o)\dot{\boldsymbol{\phi}}_o$ and $\boldsymbol{T}(\boldsymbol{\phi}_o)$ depends on the sequence of the Euler angles. The

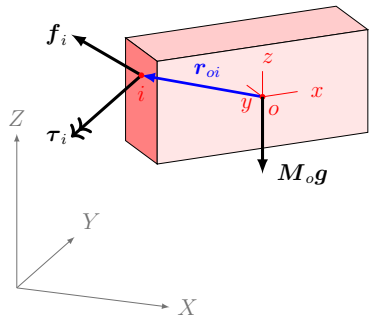

Figure 2.1: Free-body diagram of an object

dynamics of a 6-DoF object with respect to its center of mass is given by [15]:

$$\boldsymbol{M}_o(\boldsymbol{x}_o)\dot{\boldsymbol{v}}_o + \boldsymbol{C}_o(\boldsymbol{x}_o, \boldsymbol{v}_o) + \boldsymbol{g}_o(\boldsymbol{x}_o) = \boldsymbol{h}_o \tag{2.1}$$

where:

- $\boldsymbol{M}_o(\boldsymbol{x}_o) \in \mathbb{R}^{6\times6}$ is the object inertia matrix:

$$\boldsymbol{M}_o(\boldsymbol{x}_o) = \begin{bmatrix} m\boldsymbol{I}_{3\times3} & \boldsymbol{0}_{3\times3} \\ \boldsymbol{0}_{3\times3} & \boldsymbol{J}_o(\boldsymbol{x}_o) \end{bmatrix} \tag{2.2}$$

  where $\boldsymbol{J}_o(\boldsymbol{x}_o) \in \mathbb{R}^{3\times3}$ is the moment of inertia relative to the center of mass of the object, and expressed in the world frame $\{W\}$,

- $\boldsymbol{C}_o(\boldsymbol{x}_o, \boldsymbol{v}_o) \in \mathbb{R}^6$ is the Coriolis vector:

$$\boldsymbol{C}_o(\boldsymbol{x}_o, \boldsymbol{v}_o) = \begin{bmatrix} \boldsymbol{0}_{3\times1} \\ [\boldsymbol{\omega}_o]_\times \boldsymbol{J}_o \boldsymbol{\omega}_o \end{bmatrix} \tag{2.3}$$

  where $[\boldsymbol{\omega}_o]_\times \in \mathbb{R}^{3\times3}$ is the skew-symmetric matrix which is employed to replace a cross product with a matrix product,

- $\boldsymbol{g}_o(\boldsymbol{x}_o) \in \mathbb{R}^6$ is the gravity vector:

$$\boldsymbol{g}_o(\boldsymbol{x}_o) = -\boldsymbol{M}_o \boldsymbol{g} \tag{2.4}$$

  where $\boldsymbol{g} \in \mathbb{R}^6$ is the gravity vector defined with respect to the world

frame,

- $\boldsymbol{h}_o \in \mathbb{R}^6$ is the total external wrench, i.e. force and torque, applied on the object:

$$\boldsymbol{h}_o = \begin{bmatrix} \boldsymbol{f}_o \\ \boldsymbol{\tau}_o \end{bmatrix}. \tag{2.5}$$

  where $\boldsymbol{f}_o \in \mathbb{R}^3$ and $\boldsymbol{\tau}_o \in \mathbb{R}^3$ are the total external force and torque applied on the object, respectively.

Considering n_A contact points of the object with the environment and grasp positions with agents, the external wrench applied on the object is given by:

$$\boldsymbol{h}_o = \sum_{i=1}^{n_A} \boldsymbol{G}_{oi} \boldsymbol{h}_i \tag{2.6}$$

where $\boldsymbol{G}_{oi} \in \mathbb{R}^{6\times6}$ is the grasp matrix, defined as:

$$\boldsymbol{G}_{oi} = \begin{bmatrix} \boldsymbol{I}_{3\times3} & \boldsymbol{0}_{3\times3} \\ [\boldsymbol{r}_{oi}]_\times & \boldsymbol{I}_{3\times3} \end{bmatrix} \tag{2.7}$$

where $\boldsymbol{r}_{oi} \in \mathbb{R}^3$ presents the position of contact or grasp point i and $[\boldsymbol{r}_{oi}]_\times \in \mathbb{R}^{3\times3}$ is the skew-symmetric matrix which is employed to replace a cross product with a matrix product.

Finally, $\boldsymbol{h}_i \in \mathbb{R}^6$ is the external wrench applied by the agent i on the object:

$$\boldsymbol{h}_i = \begin{bmatrix} \boldsymbol{f}_i \\ \boldsymbol{\tau}_i \end{bmatrix} \tag{2.8}$$

where $\boldsymbol{f}_i \in \mathbb{R}^3$ and $\boldsymbol{\tau}_i \in \mathbb{R}^3$ are the external force and torque applied by the agent i, respectively.

2.2 Human dynamics

The human arm dynamics have been extensively studied [16]–[22] by estimating its impedance. The derivation of a dynamic model for the human arm is challenging since it is affected by several factors, such as the configuration of the arm, the state of the muscles, external forces, and the given task. Two examples of such setups for the estimation of the human arm impedance are

shown in Fig. 2.2. Despite the complexity of the experimental setup, the impedance is usually estimated using the collected external disturbance force and arm displacement.

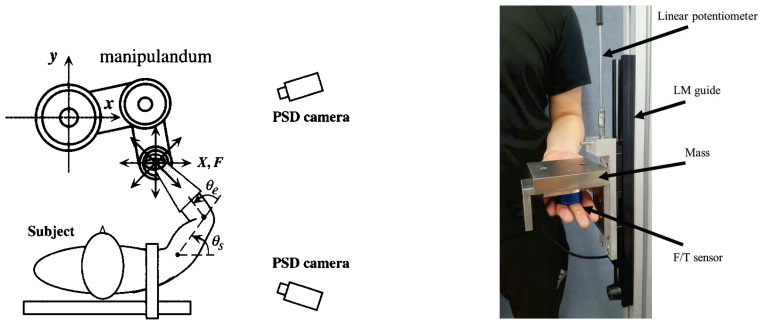

Figure 2.2: Experimental setups for estimating human arm impedance [17], [22]:
a) A manipulator applies an external displacement to the arm of the human, which is restrained, while the configuration of the arm is measured using two cameras, and the interaction force is measured using a force sensor installed at the robot end-effector [17].
b) A simple setup includes a free-falling mass and linear potentiometer for measuring the position and force/torque sensor for measuring the interaction force [22].

In this thesis, we consider a linear impedance to model the human arm, shown in Fig. 2.3. Details on such models are given in [23]. The impedance model corresponds to a spring-damper model where the rest position of the spring is the target position. By omitting the inertial effect, the linear impedance is defined as:

$$\boldsymbol{C}_h\dot{\boldsymbol{x}}_h + \boldsymbol{K}_h\tilde{\boldsymbol{x}}_h = -\boldsymbol{h}_h \tag{2.9}$$

where $\boldsymbol{C}_h \in \mathbb{R}^{6\times6}$ is the human damping gain matrix for the translational and rotational degrees of the freedom, $\boldsymbol{K}_h \in \mathbb{R}^{6\times6}$ is the human stiffness gain matrix for the translational and rotational degrees of the freedom. $\dot{\boldsymbol{x}}_h = [\dot{\boldsymbol{p}}_h^T, \dot{\boldsymbol{\phi}}_h^T]^T \in \mathbb{R}^6$ is the linear velocity and the derivative of Euler angles. $\tilde{\boldsymbol{x}}_h = [\tilde{\boldsymbol{p}}_h^T, \tilde{\boldsymbol{\phi}}_h^T]^T \in \mathbb{R}^6$ is the position error and orientation error of the human current position and their target position. Finally, $\boldsymbol{h}_h \in \mathbb{R}^6$ is the force exerted by

the human arm on the environment.

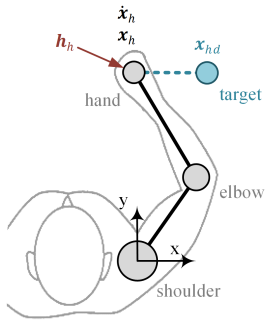

Figure 2.3: Human arm dynamics

2.3 Robot dynamics and control

The generic dynamic model of a robot arm with n joints is given by [24]:

$$\boldsymbol{B}_r(\boldsymbol{\zeta}_r)\ddot{\boldsymbol{\zeta}}_{\boldsymbol{r}} + \boldsymbol{n}_r(\boldsymbol{\zeta}_r, \dot{\boldsymbol{\zeta}}_{\boldsymbol{r}}) + \boldsymbol{g}_r(\boldsymbol{\zeta}_r) = \boldsymbol{\tau}_r - \boldsymbol{J}(\boldsymbol{\zeta}_r)^T \boldsymbol{h}_r \tag{2.10}$$

where $\boldsymbol{\zeta}_r, \dot{\boldsymbol{\zeta}}_{\boldsymbol{r}}, \ddot{\boldsymbol{\zeta}}_{\boldsymbol{r}} \in \mathbb{R}^n$ are the joint state, joint velocity and joint acceleration of the robotic system, $\boldsymbol{B}_r(\boldsymbol{\zeta}_r) \in \mathbb{R}^{n\times n}$ denotes the inertia matrix, $\boldsymbol{n}_r(\boldsymbol{\zeta}_r, \dot{\boldsymbol{\zeta}}_{\boldsymbol{r}}) \in \mathbb{R}^n$ is a vector containing the centrifugal, Coriolis and friction terms, and $\boldsymbol{g}_r(\boldsymbol{\zeta}_r) \in \mathbb{R}^n$ is the gravity vector. $\boldsymbol{\tau}_r \in \mathbb{R}^n$ is the control input to the system, $\boldsymbol{J}(\boldsymbol{\zeta}_r) \in \mathbb{R}^{6\times n}$ is the geometric Jacobian matrix and $\boldsymbol{h}_r \in \mathbb{R}^6$ is the external force and torque that the robot end-effector exerts on the environment.

For PHRC applications, it is crucial to have an appropriate interaction control scheme on robots. In the following, we briefly overview the common interaction control schemes, explained in detail in [24], [25].

- **Compliance control (Stiffness control)**: In this control scheme, the robot is set to follow a desired position and orientation, $\boldsymbol{x}_d \in \mathbb{R}^6$, while interacting with the environment. To this aim, the input torque $\boldsymbol{\tau}_r$ in (2.10) is considered as:

$$\boldsymbol{\tau}_r = \boldsymbol{g}_r(\boldsymbol{\zeta}_r) + \boldsymbol{J}_A^T(\boldsymbol{\zeta}_r)\left(\boldsymbol{K}_P \boldsymbol{\Delta x}_{dr} - \boldsymbol{K}_D \boldsymbol{J}_A(\boldsymbol{\zeta}_r)\dot{\boldsymbol{\zeta}}_r\right) \tag{2.11}$$

where $\boldsymbol{K}_P \in \mathbb{R}^{6\times6}$, $\boldsymbol{K}_D \in \mathbb{R}^{6\times6}$ are the the design parameters of controller, $\boldsymbol{\Delta x}_{dr} = \boldsymbol{x}_d - \boldsymbol{x}_r$ is the error between the desired frame and the robot end-effector frame, and $\boldsymbol{J}_A(\boldsymbol{\zeta}_r) \in \mathbb{R}^{6\times n}$ denotes the analytical Jacobian matrix. Assuming a full-rank Jacobian and substituting (2.11) in (2.10) leads to the following stable dynamics when the system is in equilibrium, i.e. $\ddot{\boldsymbol{\zeta}}_r = \dot{\boldsymbol{\zeta}}_r = 0$:

$$\boldsymbol{h}_r = \boldsymbol{T}_A^{-T}(\boldsymbol{\phi}_e)\boldsymbol{K}_P\boldsymbol{\Delta x}_{dr} \tag{2.12}$$

where

$$\boldsymbol{T}_A(\boldsymbol{\phi}_e) = \begin{bmatrix} \boldsymbol{I}_{3\times3} & \boldsymbol{0}_{3\times3} \\ \boldsymbol{0}_{3\times3} & \boldsymbol{T}(\boldsymbol{\phi}_e) \end{bmatrix}$$

and $\boldsymbol{T}(\boldsymbol{\phi}_e) \in \mathbb{R}^{3\times3}$ depends on the choice of the Euler angles set.

- **Impedance control**: This control scheme aims to decouple the dynamics of the robot, and set it to follow the desired trajectory, $\boldsymbol{x}_d$, $\dot{\boldsymbol{x}}_d$ and $\ddot{\boldsymbol{x}}_d$, and interact with the environment while keeping a desired dynamic behavior. The input torque $\boldsymbol{\tau}_r$ in (2.10) can be chosen as follows:

$$\begin{aligned}\boldsymbol{\tau}_r =& \boldsymbol{B}_r\left(\boldsymbol{J}_A^{-1}(\zeta_r)\boldsymbol{M}_{rd}^{-1}\left(\boldsymbol{M}_{rd}\ddot{\boldsymbol{x}}_{\boldsymbol{d}} + \boldsymbol{K}_D\boldsymbol{\Delta}\dot{\boldsymbol{x}}_{dr} + \boldsymbol{K}_P\boldsymbol{\Delta x}_{dr} - \boldsymbol{M}_{rd}\dot{\boldsymbol{J}}_{\boldsymbol{A}}(\zeta_r,\dot{\boldsymbol{\zeta}}_r)\dot{\boldsymbol{\zeta}}_r - \boldsymbol{h}_{rA}\right)\right) \\ &+ \boldsymbol{n}(\zeta_r,\dot{\boldsymbol{\zeta}}_r) + \boldsymbol{g}_r(\boldsymbol{\zeta}_r) + \boldsymbol{J}^T(\boldsymbol{\zeta}_r)\boldsymbol{h}_r\end{aligned} \tag{2.13}$$

where $\boldsymbol{M}_{rd} \in \mathbb{R}^{6\times6}$, $\boldsymbol{K}_P \in \mathbb{R}^{6\times6}$ and $\boldsymbol{K}_D \in \mathbb{R}^{6\times6}$ are the desired mass, damping and stiffness gain matrices, respectively, and $\boldsymbol{h}_{rA} = \boldsymbol{T}_A^T(\boldsymbol{\phi}_e)\boldsymbol{h}_r$. The control structure that can accommodate this scheme is shown in Fig. 2.4. Assuming a full-rank Jacobian, it leads to stable dynamics:

$$\boldsymbol{M}_{rd}\boldsymbol{\Delta}\ddot{\boldsymbol{x}}_{dr} + \boldsymbol{K}_D\boldsymbol{\Delta}\dot{\boldsymbol{x}}_{dr} + \boldsymbol{K}_P\boldsymbol{\Delta x}_{dr} = \boldsymbol{h}_{rA} \tag{2.14}$$

- **Admittance control**: Admittance control is designed to improve the disturbance rejection behavior of the impedance control scheme by separating motion control from impedance control. An admittance control calculates the desired position, orientation, and linear and angular velocities and accelerations of a compliant frame based on a filter that acts as an outer loop:

$$\boldsymbol{M}_{rd}\boldsymbol{\Delta}\ddot{\boldsymbol{x}}_{dc} + \boldsymbol{K}_D\boldsymbol{\Delta}\dot{\boldsymbol{x}}_{dc} + \boldsymbol{K}_P\boldsymbol{\Delta x}_{dc} = \boldsymbol{h}_r \tag{2.15}$$

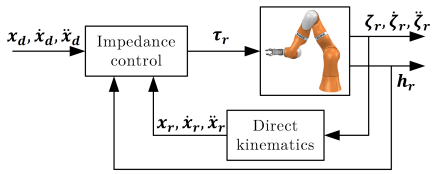

(a)

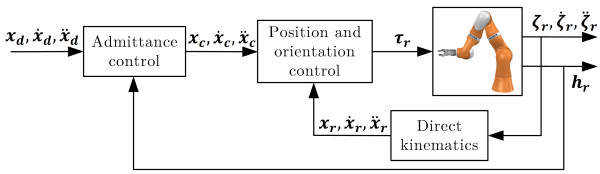

(b)

Figure 2.4: (a) Impedance and (b) Admittance control schemes

where $\boldsymbol{h}_r$ is the external wrench w.r.t. frame $\{d\}$. The scheme is shown in Fig. 2.4. The solution of (2.15) is then given as a reference to a motion controller.

Robot motion controllers do not necessarily rely on torque interfaces but can also be implemented through velocity-resolved control. Various commercial manipulators are controlled with independent proportional-integral joint velocity controllers with very high bandwidth [25]. For these robots, the closed-loop dynamics can be simplified to a first-order differential kinematic equation:

$$\dot{\boldsymbol{\zeta}}_r = \dot{\boldsymbol{\zeta}}_{ref} \tag{2.16}$$

where $\dot{\boldsymbol{\zeta}}_{ref}$ is the reference joint velocity. Thus, the input to the robot is the reference joint velocity $\dot{\boldsymbol{\zeta}}_{ref}$ instead of $\boldsymbol{\tau}_r$.

To control robots with velocity commands (2.16), a common approach is to calculate the reference velocity of the robot from the interaction force. A well-known control scheme is velocity-resolved control and can be computed

as:

$$\dot{\boldsymbol{\zeta}}_{ref} = \boldsymbol{J}_A^{-1}(\boldsymbol{\zeta}_r)\left(\dot{\boldsymbol{x}}_d + \boldsymbol{K}_D^{-1}(\boldsymbol{K}_P\boldsymbol{\Delta}\boldsymbol{x}_{dr} - \boldsymbol{h}_r)\right) \tag{2.17}$$

where $\boldsymbol{K}_D$ is the damping gain matrix and $\boldsymbol{K}_P$ is the stiffness gain matrix. Substituting (2.17) into (2.16) leads to closed-loop dynamics:

$$\boldsymbol{K}_D\boldsymbol{\Delta}\dot{\boldsymbol{x}}_{dr} + \boldsymbol{K}_P\boldsymbol{\Delta}\boldsymbol{x}_{dr} = \boldsymbol{h}_r \tag{2.18}$$

For designing an admittance control scheme for this type of robots, the desired position and velocity can be computed using (2.15) or can be computed by an outer loop that implements a simpler behavior (damping-compliance):

$$\boldsymbol{K}_D\boldsymbol{\Delta}\dot{\boldsymbol{x}}_{dc} + \boldsymbol{K}_P\boldsymbol{\Delta}\boldsymbol{x}_{dc} = \boldsymbol{h}_r \tag{2.19}$$

and sent to the inner motion controller. In case of $\boldsymbol{K}_P = \boldsymbol{0}$, the control scheme (2.19) is called damping control, and in case of $\boldsymbol{K}_D = \boldsymbol{0}$, the control scheme (2.19) is known as compliance control.

2.4 Parameter estimation

The most common method to obtain values of unknown parameters involved in dynamics is to employ the least-squares method described in the following.

Unconstrained least-squares method

Consider the following generic linear input-output (IO) model:

$$\boldsymbol{y} = \boldsymbol{\phi}\boldsymbol{\theta} \tag{2.20}$$

where $\boldsymbol{y} \in \mathbb{R}^{n_y}$ is the output and $\boldsymbol{\phi} \in \mathbb{R}^{n_y \times n_\theta}$ is the regression vector, and $\boldsymbol{\theta} \in \mathbb{R}^{n_\theta}$ is the unknown constant vector.

A classical approach to estimate the unknown parameters for a linear model is to minimize the squares of the error between the measured/known output of the system and the computed output of the model. The general form of least-squares method is in form of:

$$\hat{\boldsymbol{\theta}} = \underset{\boldsymbol{\theta}}{\operatorname{argmin}} \quad \sum_{i=1}^{N} \frac{1}{2}\gamma^{N-i}\left(\|\boldsymbol{y}_i - \boldsymbol{\phi}_i\boldsymbol{\theta}\|^2_{\boldsymbol{N}_i} + \|\boldsymbol{\theta} - \boldsymbol{\theta}_r\|^2_{\boldsymbol{W}}\right) \tag{2.21}$$

where N is the number of data, $0 < \gamma \leq 1$ is the forgetting factor, $\boldsymbol{N}_i \in \mathbb{R}^{n_y \times n_y}$ is normalization gain matrix, $\boldsymbol{\theta}_r \in \mathbb{R}^{n_\theta}$ is the leakage value, and $\boldsymbol{W} \in \mathbb{R}^{n_\theta \times n_\theta}$ is the leakage gain.

The solution of the least-squares problem (2.21) is the roots of the gradient of its cost function, i.e.:

$$\nabla_{\boldsymbol{\theta}} \left(\sum_{i=1}^{N} \frac{1}{2} \gamma^{N-i} \left(\|\boldsymbol{y}_i - \boldsymbol{\phi}_i \boldsymbol{\theta}\|^2_{\boldsymbol{N}_i} + \|\boldsymbol{\theta} - \boldsymbol{\theta}_r\|^2_{\boldsymbol{W}} \right) \right) = 0 \tag{2.22}$$

and is given by:

$$\hat{\boldsymbol{\theta}}_N = \boldsymbol{P}_N \left[\sum_{i=1}^{N} \gamma^{N-i} \left(\boldsymbol{\phi}_i^T \boldsymbol{N}_i \boldsymbol{y}_i + \boldsymbol{W} \boldsymbol{\theta}_r \right) \right] \tag{2.23}$$

where $\boldsymbol{P}_N = \left[\sum_{i=1}^{N} \gamma^{N-i} \left(\boldsymbol{\phi}_i^T \boldsymbol{N}_i \boldsymbol{\phi}_i + \boldsymbol{W} \right) \right]^{-1}$. To have a faster estimation that can produce online estimates, the solution can be written in a recursive form:

$$\hat{\boldsymbol{\theta}}_N = \hat{\boldsymbol{\theta}}_{N-1} + \boldsymbol{P}_N \left(\boldsymbol{\phi}_N^T \boldsymbol{N}_N \left(\boldsymbol{y}_N - \boldsymbol{\phi}_N \hat{\boldsymbol{\theta}}_{N-1} \right) + \boldsymbol{W} \left(\boldsymbol{\theta}_r - \hat{\boldsymbol{\theta}}_{N-1} \right) \right) \tag{2.24}$$

and

$$\boldsymbol{P}_N = \frac{1}{\gamma} \left[\boldsymbol{P}_{N-1} - \boldsymbol{P}_{N-1} \left(\boldsymbol{P}_{N-1} + \gamma \left(\boldsymbol{\phi}_N^T \boldsymbol{N}_N{}^{-1} \boldsymbol{\phi}_N + \boldsymbol{W} \right)^{-1} \right)^{-1} \boldsymbol{P}_{N-1} \right] \tag{2.25}$$

CHAPTER 3

Human Grasp Position Estimation

This chapter addresses the problem of human grasp position estimation for a scenario where the human and the robot jointly grasp an object, shown in Fig. 3.1. We derive a linear regression model with respect to the human grasp position in section 3.2. Then, the design of parameter estimators for localizing the human grasp and the challenges are discussed in section 3.3. Finally, results are presented in section 3.4.

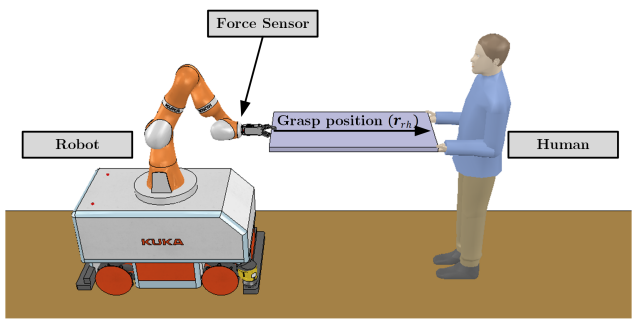

Figure 3.1: Shared object-handling scenario

3.1 Related works

Contact point estimation is a well-studied topic in robotics [13], [14]. A comprehensive review of contact detection is presented in [14]. In contact detection, it is assumed that no torque is exerted at the contact point. A sample experimental setup is shown in Fig. 3.2. Karayiannidis *et al.* [13] have also proposed an adaptive controller to estimate the contact point of the tool with the environment, along with the normal of the surface using the measured wrench at the robot end-effector. The setup is shown in Fig. 3.3

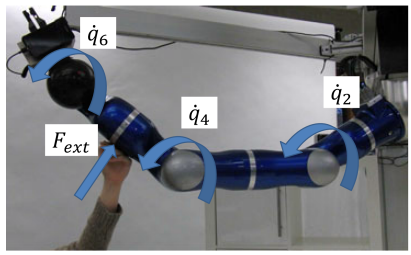

Figure 3.2: An experimental setup for collision detection [14]

Figure 3.3: Contact point estimation of a tool [13]

Similar to the contact point estimation, the human grasp point can be estimated in physical human-robot collaboration scenarios. In [26], a method for estimating the human grasp position is proposed under the assumption that the human grasp can be modeled as a passive revolute joint. The experimental setup is shown in Fig. 3.4.

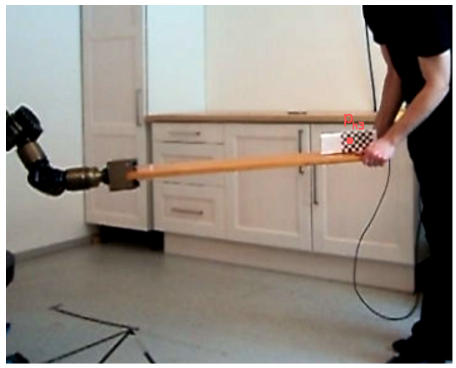

Figure 3.4: Human grasp position identification assuming that the grasp position is a passive revolute joint [26]

Human grasp position can also be estimated using motion data. In [27], the velocity and acceleration of the robot and the human are employed to estimate the human grasp position. Although the proposed estimation method does not impose any assumption on the human exerted torque, it requires additional wearable motion sensors.

In this chapter, we overview our proposed method for the estimation of the human grasp position using the measured force/torque data. Unlike [28], our method does not require any data from wearable motion sensors. Moreover, we consider the case of the "grasp" that involves simultaneous torques and forces. In the next section, we begin by formulating a linear regression for a generic object-manipulation scenario.

3.2 Problem formulation

The free-body diagram of an object interacting with a robot and a human is shown in Fig. 3.5. Using (2.1), the dynamics of the object can be written as:

$$\boldsymbol{M}_o(\boldsymbol{x}_o)\dot{\boldsymbol{v}}_o + \boldsymbol{C}_o(\boldsymbol{x}_o, \boldsymbol{v}_o) + \boldsymbol{g}_o(\boldsymbol{x}_o) = \boldsymbol{G}_{or}\boldsymbol{h}_r + \boldsymbol{G}_{oh}\boldsymbol{h}_h \tag{3.1}$$

Since all the measurements are available for the robot end-effector frame $\{R\}$, it is more convenient to derive the object dynamics with respect to this frame.

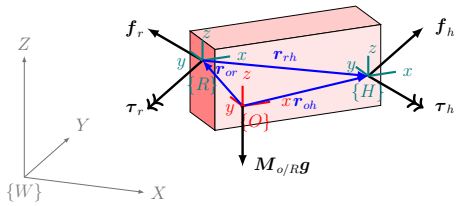

Figure 3.5: Free-body Diagram of an object

In this regard, the object dynamics can be written as:

$$\boldsymbol{M}_{o/R}\dot{\boldsymbol{v}}_{o/R} + \boldsymbol{C}_{o/R} + \boldsymbol{g}_{o/R} = \boldsymbol{h}_r + \boldsymbol{G}_{rh}\boldsymbol{h}_h \tag{3.2}$$

where

- $\boldsymbol{x}_{o/R}$ denotes the position and the orientation of the object, measured at the origin of the frame $\{R\}$, and $\boldsymbol{v}_{o/R}$ is the translational and angular velocities of the object, measured at the origin of the frame $\{R\}$,
- $\boldsymbol{M}_{o/R}$ is the object inertia matrix defined with respect to the origin of the frame $\{R\}$:

$$\boldsymbol{M}_{o/R} = \begin{bmatrix} m\boldsymbol{I}_{3\times 3} & m[\boldsymbol{r}_{or}]_\times \\ -m[\boldsymbol{r}_{or}]_\times & \boldsymbol{J}_{o/R} \end{bmatrix} \tag{3.3}$$

  where $\boldsymbol{J}_{o/R} = \boldsymbol{J}_o + m\boldsymbol{I}_{3\times 3}[r_{ro}]_\times[r_{ro}]_\times$,

- $\boldsymbol{C}_{o/R}$ is the Coriolis vector defined with respect to the origin of the frame $\{R\}$:

$$\boldsymbol{C}_{o/R} = \begin{bmatrix} -m\boldsymbol{\omega}_o \times (\boldsymbol{\omega}_o \times \boldsymbol{r}_{or}) \\ \boldsymbol{\omega}_o \times (\boldsymbol{J}_{o/R}\boldsymbol{\omega}_o) \end{bmatrix}, \tag{3.4}$$

- $\boldsymbol{g}_{o/R}$ is the gravity vector defined with respect to the origin of the frame $\{R\}$:

$$\boldsymbol{g}_{o/R} = -\boldsymbol{M}_{o/R}\boldsymbol{g}. \tag{3.5}$$

The unknown variables in the equation of motion (3.2) are the grasp position of the human, i.e. $\boldsymbol{r}_{rh}$ from the term $\boldsymbol{G}_{rh}$, and the exerted wrench by the human, i.e. $\boldsymbol{h}_h$. The human force $\boldsymbol{f}_h$ can be calculated from the translational

part of (3.2) and is given by the difference between the inertial forces and the forces measured by the sensor, $\boldsymbol{f}_r$, i.e.:

$$\boldsymbol{f}_h = \begin{bmatrix} m\boldsymbol{I}_{3\times 3} & m[\boldsymbol{r}_{or}]_\times \end{bmatrix} (\dot{\boldsymbol{v}}_{o/R} - \boldsymbol{g}) - m\boldsymbol{\omega}_o \times (\boldsymbol{\omega}_o \times \boldsymbol{r}_{or}) - \boldsymbol{f}_r. \tag{3.6}$$

Thus, we derive a parameter vector that consists of $\boldsymbol{r}_{rh}$ and $\boldsymbol{\tau}_h$:

$$\boldsymbol{\theta} \stackrel{\text{def}}{=} \begin{bmatrix} {}^R\boldsymbol{r}_{rh} \\ \boldsymbol{\tau}_h \end{bmatrix}$$

where ${}^R\boldsymbol{r}_{rh}$ is the human grasp position defined with respect to frame $\{R\}$. To identify the unknown parameters $\boldsymbol{\theta}$, the rotational part of (3.2) is written in a linear regression form as follows:

$$\boldsymbol{y} = \boldsymbol{\Phi}\boldsymbol{\theta} \tag{3.7}$$

where the known output signal $\boldsymbol{y} \in \mathbb{R}^3$ is defined as:

$$\boldsymbol{y} \stackrel{\text{def}}{=} \boldsymbol{\tau}_r - \begin{bmatrix} -m[\boldsymbol{r}_{or}]_\times & \boldsymbol{J}_{o/R} \end{bmatrix} (\dot{\boldsymbol{v}}_{o/R} - \boldsymbol{g}) - \boldsymbol{\omega}_o \times (\boldsymbol{J}_{o/R}\boldsymbol{\omega}_o) \tag{3.8}$$

and the known input signal $\boldsymbol{\Phi} \in \mathbb{R}^{3\times 6}$ is defined as:

$$\boldsymbol{\Phi} \stackrel{\text{def}}{=} \begin{bmatrix} [\boldsymbol{f}_h]_\times \boldsymbol{R}_R^W & \boldsymbol{I}_{3\times 3} \end{bmatrix} \tag{3.9}$$

where $\boldsymbol{R}_R^W$ is the rotation matrix of $\{R\}$ with respect to the world frame $\{W\}$. The identification model (3.7), combined with (3.8) and (3.9), is different from typical ones used for contact point estimation in the sense that, here, the human torque, $\boldsymbol{\tau}_h$, is considered as an unknown parameter.

3.3 Parameter estimation algorithm

Here, the goal is to estimate the human grasp position $\boldsymbol{r}_{rh}$, which is a part of the unknown parameter $\boldsymbol{\theta}$. The unconstrained least-squares method (2.21) can be employed to identify $\boldsymbol{\theta}$. The challenges for estimation of the unknown parameter $\boldsymbol{\theta}$ are listed below.

(a) The data may not contain enough information to give the possibility to solve the estimation problem. The main concept related to this problem

is the Persistence of Excitation [29]. If the input $\boldsymbol{\Phi}$ satisfies this condition, the solution of the estimator would converge to the true parameter when $N \to \infty$ [29]. However, it is challenging to satisfy this condition in real-world human-robot interaction since the excitation should be generated by the human.

(b) It is likely that human changes the grasp position to have better control over the object motion. Thus, the human grasp position may change suddenly to a new value.

(c) The human may apply torques on the object, especially if the object is grasped with two hands. Since no assumption can be made regarding the exerted torque, $\boldsymbol{\tau}_h$ is time-varying and unpredictable.

To address the mentioned challenges, we propose to modify the least-squares method with the following conditions:

- **Forgetting factor:** Since the human grasp position can change over time, we introduce a gain γ in the least-squares problem (2.21):

$$\hat{\boldsymbol{\theta}} = \underset{\boldsymbol{\theta}}{\operatorname{argmin}} \sum_{i=1}^{N} \frac{1}{2} \gamma^{N-i} \|\boldsymbol{y}_i - \boldsymbol{\Phi}_i \boldsymbol{\theta}\|^2 \tag{3.10}$$

  Choosing $\gamma = 1$ means that the old data has the same effect as the current data. Selecting $\gamma < 1$ results in reducing the effect of the old data.

- **Maximum deviation from mean:** Since variations in $\boldsymbol{\tau}_h$ and ${}^R\boldsymbol{r}_{rh}$ results in variation in the estimates, we propose to check the constancy of the estimates using the Maximum Deviation (MD) from the mean value, i.e.:

$$\mathrm{MD}(\boldsymbol{\theta}_{(t-s_{MD})\to t}) \leq \boldsymbol{E}_{cMD} \tag{3.11}$$

  where $s_{MD} \in [0, t]$. $\boldsymbol{E}_{cMD} \in \mathbb{R}^6$ is an upper bound corresponding to variables.

- **Force magnitude:** For low values of the force, the estimation problem would result in inaccurate estimation of the parameters. Thus, we disregard the data with low force magnitude.

These conditions are found by conducting an experimental study using the setup described in Section 3.4. More details on this study are given in Paper A appended in Part II. The proposed human grasp position estimation algorithm is presented in Algorithm 1, and the reader is referred to Paper A for more details.

Algorithm 1: Grasp Position Estimation Algorithm

Result: ${}^{R}\hat{\boldsymbol{r}}_{rh}$
Initialize $\boldsymbol{P}_0$, ${}^{R}\hat{\boldsymbol{r}}_{rh}$, $\hat{\boldsymbol{\theta}}$, $\boldsymbol{E}_{cMD}$, $\bar{\boldsymbol{f}}$, $\bar{\boldsymbol{r}}_{rh}$, $\underline{\boldsymbol{r}}_{rh}$;
while *(The estimator is running)* **do**
  if $\|\boldsymbol{f}_h\| > \bar{\boldsymbol{f}}$ **then**
    $\boldsymbol{P}_k = \frac{1}{\gamma}\boldsymbol{P}_{k-1} - \frac{1}{\gamma}\boldsymbol{P}_{k-1}\boldsymbol{\Phi}_k^T \left(\boldsymbol{\Phi}_k \boldsymbol{P}_{k-1}\boldsymbol{\Phi}_k^T + \gamma\right)^{-1} \boldsymbol{\Phi}_k \boldsymbol{P}_{k-1}$
    $\hat{\boldsymbol{\theta}}_k = \hat{\boldsymbol{\theta}}_{k-1} + \boldsymbol{P}_k \boldsymbol{\Phi}_k^T \left(\boldsymbol{y}_k - \Phi_k \hat{\boldsymbol{\theta}}_{k-1}\right)$
    if $\mathrm{MD}(\boldsymbol{\theta}_{(t-s_{MD})\to t}) \leq \boldsymbol{E}_{cMD}$ **then**
      ${}^{R}\hat{\boldsymbol{r}}_{rh} = \min(\bar{\boldsymbol{r}}_{rh}, \max(\underline{\boldsymbol{r}}_{rh}, \hat{\boldsymbol{\theta}}_{k,1:3}))$
    end
    $k \leftarrow k+1$
  end
end

3.4 Experimental results

For evaluation of the proposed Algorithm 1, a set of data is collected using the experimental setup, shown in Fig. 3.6. The setup includes a UR10 collaborative robot, two OptoForce force/torque sensors, and a light-weight aluminum object. The motion data is collected using the software of UR10 robot, and the force data is also collected through the force/torque sensors. The robot-side wrench data, collected using the robot-side force sensor, is given to the estimation Algorithm 1, and the human-side wrench data, collected using the human-side force sensor, is used for validation.

To demonstrate the performance of the proposed estimation Algorithm 1, two scenarios are considered here. The main objective of considering these scenarios is evaluating the effect of applied torque on the estimation of the grasp position.

(a) **Scenario A** demonstrates the situation that human applies constant

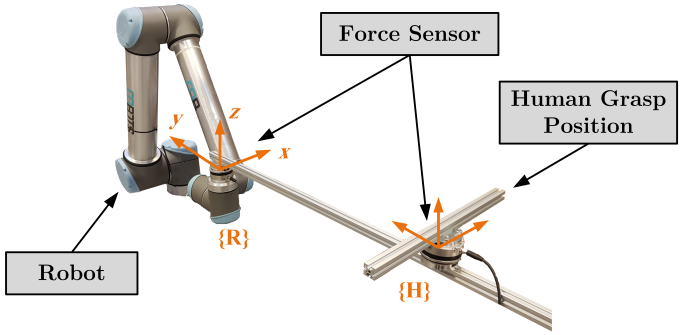

Figure 3.6: Experimental setup for collecting data

torque. The human applied force and torque are shown in Fig. 3.7. $\boldsymbol{\tau}_h$ has low variances in three different time intervals, $[3, 13]$, $[14, 30]$ and $[31, 43]$ (s). ${}^R\hat{\boldsymbol{r}}_{rh}$ along with the true human grasp position are depicted in Fig. 3.8. In the time interval $[0, 5]$ (s), the estimations of the position vary about 1 meter, where the final estimation ${}^R\hat{\boldsymbol{r}}_{rh}$ stays at its initial values. After that, the maximum deviation condition is satisfied, ${}^R\hat{\boldsymbol{r}}_{rh}$ updates to the estimated value $\hat{\boldsymbol{\theta}}_{1:3}$ which is close to the true value of the grasp point. Then, the human changes the grasp position twice at 14 s and 29 s. In both cases, the estimator updates the human grasp position, ${}^R\hat{\boldsymbol{r}}_{rh}$, after about 3 s delay to a value close to the true grasp position.

(b) **Scenario B** demonstrates the robustness of the algorithm with respect to incorrect estimations. The applied force and torque of the human are shown in Fig. 3.9. The value of $\boldsymbol{\tau}_h$ is time-varying between 18 s and 44 s. The estimation results are shown in Fig. 3.10. The estimates $\hat{\boldsymbol{\theta}}$ generated by the main estimator vary while the human torque is exerted. However, since the estimates are not constant, the maximum deviation from the mean condition (3.11) is not satisfied and consequently, the final estimation ${}^R\hat{\boldsymbol{r}}_{rh}$ does not get updated.

More scenarios, as well as the evaluation of the proposed approach based on the experimental data, can be found in Paper A.

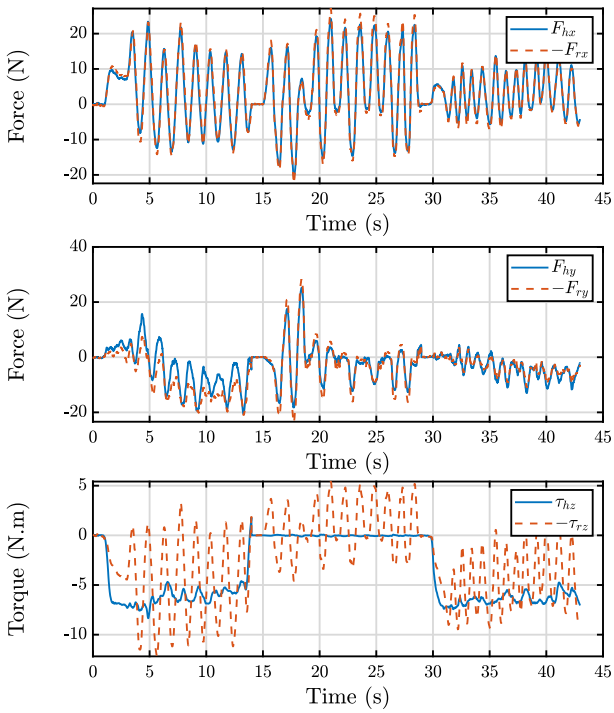

Figure 3.7: Applied forces and torque by the human and the reaction forces and torque measured by the robot for scenario A

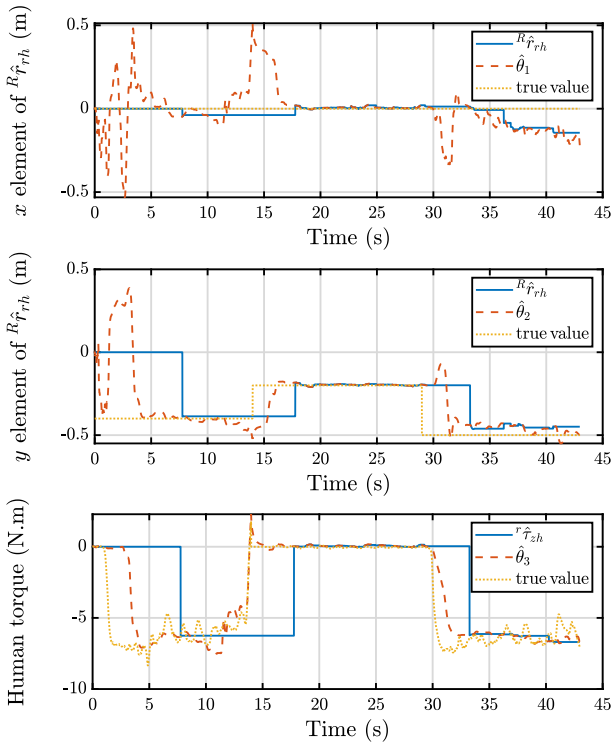

Figure 3.8: Human grasp position estimation for scenario A

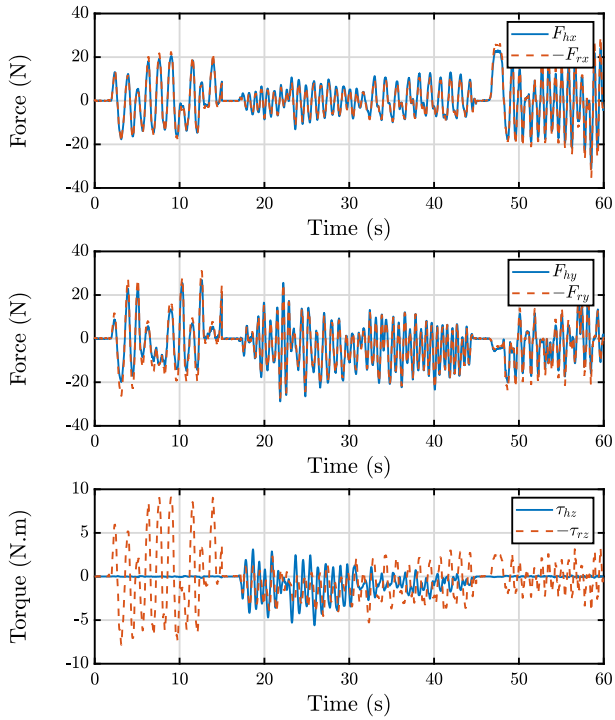

Figure 3.9: Applied forces and torque by the human and the reaction forces and torque measured by the robot for scenario B

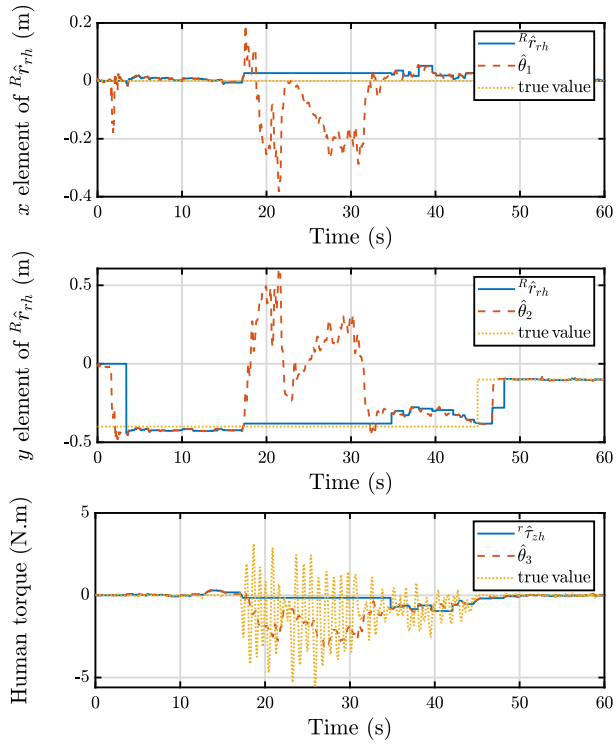

Figure 3.10: Human grasp position estimation for scenario B

CHAPTER 4

Shared Object Manipulation, Dynamics and Control

This chapter provides the derivation of the interaction dynamics for a typical PHRC scenario, shown in Fig. 4.1, and discusses the design of a control scheme for the robot in order to reduce the effort of the human while rotating and translating the object. In section 4.1, we present an overview of related works, particularly those referring to the translation/rotation problem. In section 4.2, we derive the interaction dynamics in order to formally introduce the translation/rotation problem in section 4.3 and evaluate control strategies to deal with this problem. Overview of our proposed control scheme is given in section 4.4.

4.1 Related works

The study of the interaction dynamics of cooperative robotic systems has been the subject of many classic and recent studies [30]–[33].

Erhart et al. [33] propose a new approach to model the interaction dynamics and derive the explicit solution of the interaction wrenches for a cooperative manipulation task. Moreover, they derive the impedance characteristic of the cooperative system that appears in response to an external disturbance.

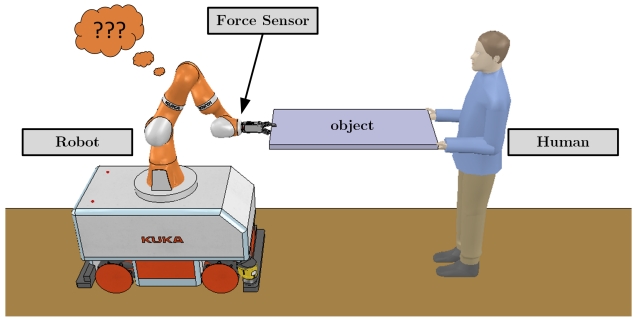

Figure 4.1: Shared object-handling scenario

The interaction wrenches can be employed to interpret the intention of the human. In case of direct interaction with the robot, the intention of the human is clear from the wrench measurements. However, in case of an object between the human and robot, i.e., measuring human force indirectly, the intention of the human becomes ambiguous. Dumora et al. [34] investigated the detection of the human intention of motion by exploiting haptic cues through an experimental study. Measuring human wrench indirectly using the force/torque sensor installed at the robot grasp position, they reported that human intention for lateral translation is indistinguishable from the intention for pure rotation. Thus, designing control schemes to generate robotic motion based on the intention of the human becomes challenging.

Adding a virtual non-holonomic constraint to the controller does not contribute to human intention detection, but could facilitate the manipulation of the object. The proposed method in [35] employs a nonholonomic constraint at the robot end-effector. Although the control scheme is free of switching policies and independent of the object geometry, it confines the object transportation to some degrees of freedom.

Karayiannidis et al. [36] propose to employ the measured force at the robot end-effector to switch between two constrained motions, i.e., object translation or object rotation. Various switching policies are evaluated, and the force magnitude is selected as an indicator of the human intention. However, this method works satisfactorily for slow rotations or fast translations and cannot support rich motions, including combined translations and rotations.

In another study, [37], a fixture including free joints equipped with en-

coders, and a dedicated torque sensor at the grasp position, are employed to accomplish a cooperative assembly task. Displacement information derived from the free joints, complement the force data to design a controller that allows independent translational and rotational motions. However, designing a fixture and installing different sensors limit the application of the proposed controller.

Here, we propose a control scheme that allows the human to move the object in all degrees of freedom while it does not require an additional modification of the object. This is achieved by assuming that the human grasp position is known. In the next section, we begin by deriving the interaction dynamics.

4.2 Interaction dynamics of shared object manipulation

The free-body diagram of an object for a planar PHRI scenario is shown in Fig. 4.2. Deriving the interaction dynamics for this scenario requires studying the dynamics of the object, the robot, and the human.

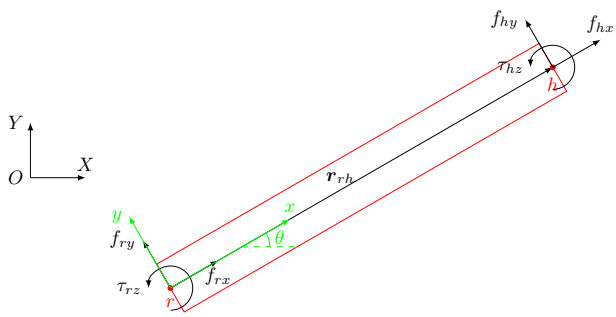

Figure 4.2: Free-body diagram of the object for a planar PHRI scenario

Object dynamics

To focus on the distance between the human grasp position and the robot grasp position, the object inertia is ignored, i.e.:

Assumption 1. *The object is lightweight, i.e.* $\boldsymbol{M}_o \approx \boldsymbol{0}$ *and* $\boldsymbol{J}_o \approx \boldsymbol{0}$.

Furthermore, it is assumed that the human grasps the object at the position ${}^R\boldsymbol{r}_{rh} = [l, 0]^T$. Using the assumptions, the object dynamics (2.1) simplifies to:

$$\begin{bmatrix} {}^Rf_{rx} \\ {}^Rf_{ry} \\ \tau_{rz} \end{bmatrix} = - \begin{bmatrix} {}^Rf_{hx} \\ {}^Rf_{hy} \\ l{}^Rf_{hy} + \tau_{hz} \end{bmatrix} \tag{4.1}$$

Robot dynamics

The first-order differential kinematic in form of (2.16) along with the damping control in form of (2.19) is considered for the robot. The closed-loop dynamics of the robot is given by:

$$\begin{bmatrix} c_{rvx} & 0 & 0 \\ 0 & c_{rvy} & 0 \\ 0 & 0 & c_{r\omega z} \end{bmatrix} \begin{bmatrix} {}^R\dot{p}_{rx} \\ {}^R\dot{p}_{ry} \\ \omega_{rz} \end{bmatrix} = - \begin{bmatrix} {}^Rf_{rx} \\ {}^Rf_{ry} \\ \tau_{rz} \end{bmatrix} \tag{4.2}$$

where c_{rvx}, c_{rvy} and $c_{r\omega z}$ are the admittance controller gain for the translational movements along x- and y-axis and rotational movement around z-axis, respectively. ${}^R\dot{p}_{rx}$, ${}^R\dot{p}_{ry}$ and ω_{rz} are the linear velocities along x- and y-axis and the angular velocity of the robot around z-axis. Depending on the selection of the translational and rotational gains of the admittance controller, different modes of control can be achieved. For example, by selecting c_{rvx} and c_{rvy} high enough, the robot would be in a rotation mode around its end-effector, and by selecting $c_{r\omega z}$ high enough, the rotation of the end-effector can be locked.

Human dynamics

Using (2.9), the impedance model of human arm dynamics for a planar motion (3-DoF) is given by:

$$\begin{bmatrix} c_{hvx} & 0 & 0 \\ 0 & c_{hvy} & 0 \\ 0 & 0 & c_{h\omega z} \end{bmatrix} \begin{bmatrix} {}^R\dot{p}_{hx} \\ {}^R\dot{p}_{hy} \\ \omega_{hz} \end{bmatrix} + \begin{bmatrix} k_{hvx} & 0 & 0 \\ 0 & k_{hvy} & 0 \\ 0 & 0 & k_{h\omega z} \end{bmatrix} \begin{bmatrix} {}^R\tilde{p}_{hx} \\ {}^R\tilde{p}_{hy} \\ \tilde{\theta}_{hz} \end{bmatrix} = - \begin{bmatrix} {}^Rf_{hx} \\ {}^Rf_{hy} \\ \tau_{hz} \end{bmatrix} \tag{4.3}$$

where c_{hvx}, c_{hvy} and $c_{h\omega z}$ are the human damping gains and k_{hvx}, k_{hvy} and $k_{h\omega z}$ are the human stiffness gains along x- and y-direction and about z-axis, respectively. ${}^{R}\dot{p}_{hx}$, ${}^{R}\dot{p}_{hy}$ and ω_{hz} are the linear velocities along x- and y-axis and the angular velocity of the human arm around z-axis. ${}^{R}\tilde{p}_{hx}$, ${}^{R}\tilde{p}_{hy}$ and $\tilde{\theta}_{hz}$ are the translational and rotational errors between the current human position and their desired position.

Constraints

Since the human and the robot are grasping the same object, they cannot move independently. In this regard, the following assumption is made:

Assumption 2. *The object, as well as the connections between the object and the agents, i.e., human and robot, are assumed to be rigid.*

Due to the rigidity of the connections, both translational and rotational motions are restricted. This limitation of the movement can be formulated through kinematic constraints. These constraints are defined as follows:

$$\begin{cases} p_{hx} = p_{rx} + l\cos\theta \\ p_{hy} = p_{ry} + l\sin\theta \\ \theta_h = \theta_r \end{cases} \tag{4.4}$$

which leads to the following velocity constraints:

$$\begin{cases} {}^{R}\dot{p}_{hx} = {}^{R}\dot{p}_{rx} \\ {}^{R}\dot{p}_{hy} = {}^{R}\dot{p}_{ry} + l\omega \\ \omega_h = \omega_r \end{cases} \tag{4.5}$$

Interaction dynamics

The dynamics of the object (4.1) and the agents (4.2) and (4.3) are coupled through the kinematic constraints (4.5). The dynamics of the coupled system with respect to the human velocity is derived by solving these equations for unknown variables ${}^{R}\dot{p}_{hx}$, ${}^{R}\dot{p}_{hy}$, ω_{hz}, ${}^{R}\dot{p}_{rx}$, ${}^{R}\dot{p}_{ry}$, ω_{rz} and ${}^{R}f_{hx}$, ${}^{R}f_{hy}$, τ_{hz},

${}^{R}f_{rx}$, ${}^{R}f_{ry}$ and τ_{rz}, and can be written as:

$$\begin{bmatrix} c_{rvx}+c_{hvx} & 0 & 0 \\ 0 & c_{rvy}+c_{hvy} & -c_{rvy}l \\ 0 & -c_{rvy}l & c_{h\omega z}+c_{r\omega z}+c_{rvy}l^2 \end{bmatrix} \begin{bmatrix} {}^{R}\dot{p}_{hx} \\ {}^{R}\dot{p}_{hy} \\ \omega_{hz} \end{bmatrix} = \begin{bmatrix} -k_{hvx}{}^{R}\tilde{p}_{hx} \\ -k_{hvy}{}^{R}\tilde{p}_{hy} \\ -k_{h\omega z}\tilde{\theta}_{hz} \end{bmatrix} \tag{4.6}$$

Moreover, the interaction forces and torque, ${}^{R}f_{hx}$, ${}^{R}f_{hy}$ and τ_{hz} are given by the following closed form expression:

$$\begin{cases} {}^{R}f_{hx} = \dfrac{-c_{rvx}k_{hvx}{}^{R}\tilde{p}_{hx}}{c_{hvx}+c_{rvx}} \\ {}^{R}f_{hy} = \dfrac{-c_{rvy}(c_{r\omega z}+c_{h\omega z})k_{hvy}{}^{R}\tilde{p}_{hy}+c_{hvy}c_{rvy}lk_{h\omega z}\tilde{\theta}_{hz}}{(c_{rvy}+c_{hvy})(c_{r\omega z}+c_{h\omega z})+c_{hvy}c_{rvy}l^2} \\ \tau_{hz} = \dfrac{c_{h\omega z}c_{rvy}k_{hvy}l{}^{R}\tilde{p}_{hy}-(c_{hvy}c_{r\omega z}+c_{rvy}c_{r\omega z}+c_{hvy}c_{rvy}l^2)k_{hwz}\tilde{\theta}_{hz}}{(c_{rvy}+c_{hvy})(c_{r\omega z}+c_{h\omega z})+c_{hvy}c_{rvy}l^2} \end{cases} \tag{4.7}$$

Eq. (4.7) shows how the interaction forces, ${}^{R}f_{hx}$ and ${}^{R}f_{hy}$, and the interaction torque τ_{hz} are related to the human error ${}^{R}\tilde{p}_{hx}$, ${}^{R}\tilde{p}_{hy}$ and $\tilde{\theta}_{hz}$. It can be seen that the force along y-direction, ${}^{R}f_{hy}$, is a function of the errors along y-direction and about z-direction, i.e. ${}^{R}\tilde{p}_{hy}$ and $\tilde{\theta}_{hz}$. Similarly, τ_{hz} is a function of ${}^{R}\tilde{p}_{hy}$ and $\tilde{\theta}_{hz}$. In case of $l = 0$, i.e. no distance between the robot and the human, (4.7) simplifies to:

$$\begin{cases} {}^{R}f_{hx} = \dfrac{-c_{rvx}k_{hvx}{}^{R}\tilde{p}_{hx}}{c_{hvx}+c_{rvx}} \\ {}^{R}f_{hy} = \dfrac{-c_{rvy}k_{hvy}{}^{R}\tilde{p}_{hy}}{c_{rvy}+c_{hvy}} \\ \tau_{hz} = \dfrac{-c_{r\omega z}k_{hwz}\tilde{\theta}_{hz}}{c_{r\omega z}+c_{h\omega z}} \end{cases} \tag{4.8}$$

Eq. (4.8) implies that ${}^{R}f_{hx}$, ${}^{R}f_{hy}$ and τ_{hz} are directly related to the corresponding translational and rotational errors, given by ${}^{R}\tilde{p}_{hx}$, ${}^{R}\tilde{p}_{hy}$ and $\tilde{\theta}_{hz}$, and are independent of errors in other dimensions. This implies a closed-loop decoupled behavior where the forces of the operator yield to motion only along with the corresponding directions. In other words, the intention of the

operator for moving the object can be clearly observed from the forces. However, in case of $l \neq 0$, the relation between human forces and position errors becomes coupled and more complicated, leading to the Translation/Rotation problem.

4.3 Translation/Rotation problem

In case of $l \neq 0$, (4.7) implies that ${}^{R}f_{hy}$ and τ_{hz} are affected by both ${}^{R}\tilde{p}_{hy}$ and $\tilde{\theta}_{hz}$. A cross effect can be seen between two dimensions, i.e., a term including $\tilde{\theta}_{hz}$ exists in the force along the y axis and another term including ${}^{R}\tilde{p}_{hy}$ exists in the torque about the z axis, which means that the intention of the human cannot be observed from the applied force. In other words, the distance between the human and the force sensor, l, obscures the human intention. This cross effect yields the translation/rotation problem.

Takubu et al. [35] proposed to utilize the simple admittance controller with a nonholonomic constraint to avoid translation/rotation problem. The effect of this nonholonomic admitance controller can be seen by substituting $c_{rvy} \to \infty$ in the interaction dynamics (4.7):

$$\begin{cases} {}^{R}f_{hx} = \dfrac{-c_{rvx}k_{hvx}{}^{R}\tilde{p}_{hx}}{c_{hvx} + c_{rvx}} \\ {}^{R}f_{hy} = \dfrac{-(c_{r\omega z} + c_{h\omega z})k_{hvy}{}^{R}\tilde{p}_{hy} + c_{hvy}lk_{h\omega z}\tilde{\theta}_{hz}}{c_{r\omega z} + c_{h\omega z} + c_{hvy}l^2} \\ \tau_{hz} = \dfrac{c_{h\omega z}k_{hvy}l{}^{R}\tilde{p}_{hy} - (c_{r\omega z} + c_{hvy}l^2)k_{hwz}\tilde{\theta}_{hz}}{c_{r\omega z} + c_{h\omega z} + c_{hvy}l^2} \end{cases} \tag{4.9}$$

Although this method resolves the translation/rotation problem, it limits the motion of the object. Moreover, it can be seen that ${}^{R}f_{hy}$ and τ_{hz} are still affected by both ${}^{R}\tilde{p}_{hy}$ and $\tilde{\theta}_{hz}$.

Karayiannidis et al. [36] proposed to employ two different modes for the controller, namely, translation mode and rotation mode. In the translation mode, the human can just perform a translation of the object, and in the rotation mode, the human can rotate the object around the robot end-effector. The condition for switching between the modes is based on the magnitude of the force. Moreover, it is assumed that the human could just apply forces on the object, i.e., $k_{h\omega z} = 0$ and $c_{h\omega z} = 0$, which result in $\tau_{hz} = 0$.

The interaction forces for the rotation mode can be derived by setting

$c_{rvx} \to \infty$ and $c_{rvy} \to \infty$ in the interaction dynamics (4.7):

$$\begin{cases} {}^{R}f_{hx} = -k_{hvx}\,{}^{R}\tilde{p}_{hx} \\ {}^{R}f_{hy} = \dfrac{-(c_{r\omega z} + c_{h\omega z})k_{hvy}\,{}^{R}\tilde{p}_{hy} + c_{hvy}lk_{h\omega z}\tilde{\theta}_{hz}}{c_{r\omega z} + c_{h\omega z} + c_{hvy}l^2} \\ \tau_{hz} = 0 \end{cases} \tag{4.10}$$

and the equations for the translation mode is computed by setting $c_{r\omega z} \to \infty$:

$$\begin{cases} {}^{R}f_{hx} = -\dfrac{c_{rvx}k_{hvx}\,{}^{R}\tilde{p}_{hx}}{c_{hvx} + c_{rvx}} \\ {}^{R}f_{hy} = -\dfrac{c_{rvy}k_{hvy}\,{}^{R}\tilde{p}_{hy}}{c_{hvy} + c_{rvy}} \\ \tau_{hz} = 0 \end{cases} \tag{4.11}$$

In the translation mode, a decoupled behaviour is achieved similar to the closed-loop dynamics (4.8). However, in the rotation mode ${}^{R}f_{hy}$ is affected by both ${}^{R}\tilde{p}_{hy}$ and $\tilde{\theta}_{hz}$, similar to closed-loop dynamics (4.9). Moreover, the human force ${}^{R}f_{hy}$ is dependent on the length l between the robot and the human.

4.4 Controller design

To avoid the translation/rotation problem, we propose to translate and rotate the object relative to the human applied force and torque, respectively. Let us define a new frame $\{C\}$, located at the human grasp position (Fig. 4.3a), as a reference frame for defining the velocity command. To have a one-to-one relation between the applied wrench and velocities of the object at the origin of frame $\{C\}$, we define the following dynamics:

$$\begin{bmatrix} c_{rvx} & 0 & 0 \\ 0 & c_{rvy} & 0 \\ 0 & 0 & c_{r\omega z} \end{bmatrix} \begin{bmatrix} {}^{R}\dot{p}_{Cx} \\ {}^{R}\dot{p}_{Cy} \\ \omega_C \end{bmatrix} = \begin{bmatrix} {}^{R}f_{hx} \\ {}^{R}f_{hy} \\ \tau_{hz} \end{bmatrix} \tag{4.12}$$

where ${}^R\dot{p}_{Cx}$ and ${}^R\dot{p}_{Cy}$ are the translational velocities along axes x and y, and ω_C is the angular velocity around axis z. Note that the wrench applied by the human, i.e., $[{}^R f_{hx}, {}^R f_{hy}, \tau_{hz}]^T$, is not available through direct measurements and for its accurate derivation a known human grasp position is assumed. In the considered scenario, it is equivalent to a known value of l. Using (4.1), (4.5), and the controller (4.12), the velocity command for the robot is derived as follows:

$$\begin{bmatrix} {}^R\dot{p}_{rx} \\ {}^R\dot{p}_{ry} \\ \omega_r \end{bmatrix} = \begin{bmatrix} 1 & 0 & 0 \\ 0 & 1 & l \\ 0 & 0 & 1 \end{bmatrix}^{-1} \begin{bmatrix} c_{rvx} & 0 & 0 \\ 0 & c_{rvy} & 0 \\ 0 & 0 & c_{r\omega z} \end{bmatrix}^{-1} \begin{bmatrix} -1 & 0 & 0 \\ 0 & -1 & 0 \\ 0 & l & -1 \end{bmatrix} \begin{bmatrix} {}^R f_{rx} \\ {}^R f_{ry} \\ \tau_{rz} \end{bmatrix} \tag{4.13}$$

which leads to the following interaction wrenches:

$$\begin{cases} {}^R f_{hx} = \dfrac{-c_{rvx} k_{hvx} {}^R\tilde{p}_{hx}}{c_{hvx} + c_{rvx}} \\ {}^R f_{hy} = \dfrac{-c_{rvy} k_{hvy} {}^R\tilde{p}_{hy}}{c_{rvy} + c_{hvy}} \\ \tau_{hz} = \dfrac{-c_{r\omega z} k_{hwz} \tilde{\theta}_{hz}}{c_{r\omega z} + c_{h\omega z}} \end{cases} \tag{4.14}$$

The interaction wrenches of the human in (4.14) are related only to the corresponding position errors, and thus the proposed controller can be used to avoid the couplings resulting from translation/rotation problem.

Based on the concept of the "instantaneous center of zero velocity" [15], the object can be considered to be in pure rotation about an axis, normal to the plane of motion. Thus, the translational and rotational motion generated by the dynamics (4.12) can also be considered as a pure rotation with the same angular velocity, ω_C, about a different axis. This means that by changing the position of the frame $\{C\}$, the same torque can be used to produce the same motion without requiring any force applied on the object (Fig. 4.3b). To dynamically modify the origin point of the frame $\{C\}$ towards the instantaneous center of rotation, we propose an adaptive control scheme. The control is based on the measured forces and torque at the robot side and is explained in detail in Paper B appended in Part II.

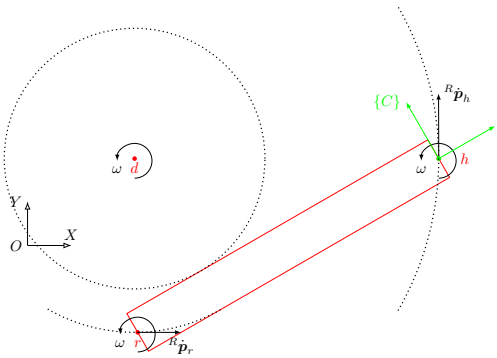

(a)

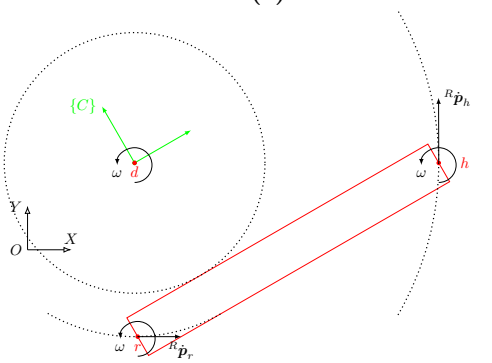

(b)

Figure 4.3: Rotation of the object around the instantaneous center of zero velocity d. (a) The frame $\{C\}$ is located at human grasp position and controller (4.13) is employed for generating velocity commands. (b) By locating the frame $\{C\}$ at the instantaneous center of rotation, the same motion can be generated using the human applied torque.

CHAPTER 5

Contributions and Future Works

5.1 Contributions

In the previous chapters, we reviewed the methods and models used for a cooperative object-manipulation scenario in PHRC. In this chapter, the summary of the appended papers in part II is presented. Besides, possible future research directions are briefly discussed.

Paper A

Haptic sensing and analysis of interaction wrenches are crucial for developing effective collaboration between humans and robots. The focus of this paper is on estimating the grasp position of the human for human-robot collaborative object manipulation. While many studies consider no external torque for contact, in this paper, we explicitly take into account the effect of the human applied torque to localize the human grasp and evaluate the validity of the estimates. In our approach, conventional estimation methods are utilized, and appropriate conditions are checked to estimate the human grasp position. The human grasp position estimation method is also investigated experimentally. Using the experimental data, we assess different criteria to dismiss unreliable estimates. The proposed model is then evaluated by comparing it with a

conventional contact point identification model. The performance of the proposed algorithm is also verified through 4 scenarios considering the presence of human applied torque. The results show that the conventional contact point estimation is not accurate for the generic case of human grasp, and the proposed grasp point estimation is more robust and accurate for estimating the human grasp position.

Paper B

In this paper, we develop a control scheme to overcome the translation/rotation problem in a shared object manipulation scenario. The idea is to move the robot in a way that the grasp position of the human moves proportional to the applied force and torque by the human. To implement this, we assume a known location for the human grasp. Furthermore, by employing the concept of zero velocity center, we propose an update rule to reduce the effort of the human. The introduced controller reduces the effort by decreasing the applied force of the human. In addition, the passivity of the closed-loop system, including the robot manipulator and the object, and the convergence of the controller reference point to the zero velocity center, are proved theoretically. Finally, the performance of the new control scheme is demonstrated through simulation scenarios.

5.2 Future works

The thesis considers the human grasp position estimation and object handling problems individually. The limitation of the control scheme proposed in Paper B is the assumption that the human grasp position is known, which can be alleviated using the method proposed in Paper A. In this regard, first, we will combine both methods as an indirect adaptive control scheme using the certainty equivalence principle. The human grasp position will be provided by the estimator and will be used as the true grasp position in the control scheme. We will then evaluate the robustness of the controller with respect to the uncertainty of the human grasp position and also address the safety of the human during the interaction. We will also consider a direct adaptive control scheme and compare the two approaches. Furthermore, we will design appropriate interaction scenarios to conduct human studies. Besides performance metrics, we will also consider quantitative and qualitative results from different users interacting with the robot.

References

[1] G. Michalos, S. Makris, J. Spiliotopoulos, I. Misios, P. Tsarouchi, and G. Chryssolouris, "Robo-partner: Seamless human-robot cooperation for intelligent, flexible and safe operations in the assembly factories of the future", *Procedia CIRP*, vol. 23, pp. 71–76, 2014.

[2] R. R. Murphy, D. Riddle, and E. Rasmussen, "Robot-assisted medical reachback: A survey of how medical personnel expect to interact with rescue robots", in *RO-MAN 2004. 13th IEEE International Workshop on Robot and Human Interactive Communication (IEEE Catalog No. 04TH8759)*, IEEE, 2004, pp. 301–306.

[3] W. Bluethmann, R. Ambrose, M. Diftler, S. Askew, E. Huber, M. Goza, F. Rehnmark, C. Lovchik, and D. Magruder, "Robonaut: A robot designed to work with humans in space", *Autonomous robots*, vol. 14, no. 2-3, pp. 179–197, 2003.

[4] J. Pineau, M. Montemerlo, M. Pollack, N. Roy, and S. Thrun, "Towards robotic assistants in nursing homes: Challenges and results", *Robotics and autonomous systems*, vol. 42, no. 3-4, pp. 271–281, 2003.

[5] A. Ajoudani, A. M. Zanchettin, S. Ivaldi, A. Albu-Schäffer, K. Kosuge, and O. Khatib, "Progress and prospects of the human–robot collaboration", *Autonomous Robots*, pp. 1–19, 2018.

[6] D. P. Losey, C. G. McDonald, E. Battaglia, and M. K. O'Malley, "A review of intent detection, arbitration, and communication aspects of

shared control for physical human–robot interaction", *Applied Mechanics Reviews*, vol. 70, no. 1, p. 010 804, 2018.

[7] "Robots and robotic devices — Collaborative robots", International Organization for Standardization, Geneva, Standard ISO/TS 15066:2016, 2016.

[8] V. Villani, F. Pini, F. Leali, and C. Secchi, "Survey on human–robot collaboration in industrial settings: Safety, intuitive interfaces and applications", *Mechatronics*, vol. 55, pp. 248–266, 2018.

[9] M. A. Goodrich, A. C. Schultz, *et al.*, "Human–robot interaction: A survey", *Foundations and Trends® in Human–Computer Interaction*, vol. 1, no. 3, pp. 203–275, 2008.

[10] T. B. Sheridan, "Human–robot interaction: Status and challenges", *Human factors*, vol. 58, no. 4, pp. 525–532, 2016.

[11] "Collaborative robot market by payload capacity (up to 5 kg, between 5 and 10 kg, above 10 kg), industry (automotive, electronics, metals & machining, plastics & polymers, food & beverages, healthcare), application, and geography - global forecast to 2025", MarketsandMarkets, Tech. Rep., 2018.

[12] A. Sharma. (2019). The future of collaborative robots, [Online]. Available: `https://www.interactanalysis.com/collaborative-robots/`.

[13] Y. Karayiannidis, C. Smith, F. E. Vina, and D. Kragic, "Online contact point estimation for uncalibrated tool use", in *2014 IEEE International Conference on Robotics and Automation (ICRA)*, IEEE, 2014, pp. 2488–2494.

[14] S. Haddadin, A. De Luca, and A. Albu-Schäffer, "Robot collisions: A survey on detection, isolation, and identification", *IEEE Transactions on Robotics*, vol. 33, no. 6, pp. 1292–1312, 2017.

[15] J. L. Meriam and L. G. Kraige, *Engineering mechanics: dynamics*. John Wiley & Sons, 2012, vol. 2.

[16] J. M. Dolan, M. B. Friedman, and M. L. Nagurka, "Dynamic and loaded impedance components in the maintenance of human arm posture", *IEEE Transactions on Systems, Man, and Cybernetics*, vol. 23, no. 3, pp. 698–709, 1993.

[17] T. Tsuji, P. G. Morasso, K. Goto, and K. Ito, "Human hand impedance characteristics during maintained posture", *Biological cybernetics*, vol. 72, no. 6, pp. 475–485, 1995.

[18] M. Rahman, R. Ikeura, and K. Mizutani, "Investigating the impedance characteristic of human arm for development of robots to co-operate with human operators", in *IEEE SMC'99 Conference Proceedings. 1999 IEEE International Conference on Systems, Man, and Cybernetics (Cat. No. 99CH37028)*, IEEE, vol. 2, 1999, pp. 676–681.

[19] K. P. Tee, E. Burdet, C.-M. Chew, and T. E. Milner, "A model of force and impedance in human arm movements", *Biological cybernetics*, vol. 90, no. 5, pp. 368–375, 2004.

[20] F. Mobasser and K. Hashtrudi-Zaad, "A method for online estimation of human arm dynamics", in *2006 International Conference of the IEEE Engineering in Medicine and Biology Society*, IEEE, 2006, pp. 2412–2416.

[21] I. Tejado, D. Valério, P. Pires, and J. Martins, "Fractional order human arm dynamics with variability analyses", *Mechatronics*, vol. 23, no. 7, pp. 805–812, 2013.

[22] K. H. Lee, S. G. Baek, H. J. Lee, H. R. Choi, H. Moon, and J. C. Koo, "Enhanced transparency for physical human-robot interaction using human hand impedance compensation", *IEEE/ASME Transactions on Mechatronics*, vol. 23, no. 6, pp. 2662–2670, 2018.

[23] M. S. Erden and A. Billard, "End-point impedance measurements across dominant and nondominant hands and robotic assistance with directional damping", *IEEE transactions on cybernetics*, vol. 45, no. 6, pp. 1146–1157, 2014.

[24] B. Siciliano, L. Sciavicco, L. Villani, and G. Oriolo, *Robotics: modelling, planning and control*. Springer Science & Business Media, 2010.

[25] B. Siciliano and O. Khatib, *Springer handbook of robotics*. Springer, 2016.

[26] Y. Karayiannidis, C. Smith, F. E. Vina, and D. Kragic, "Online kinematics estimation for active human-robot manipulation of jointly held objects", in *2013 IEEE/RSJ International Conference on Intelligent Robots and Systems*, IEEE, 2013, pp. 4872–4878.

[27] D. Ćehajić, P. B. g. Dohmann, and S. Hirche, "Estimating unknown object dynamics in human-robot manipulation tasks", in *2017 IEEE International Conference on Robotics and Automation (ICRA)*, IEEE, 2017, pp. 1730–1737.

[28] D. Ćehajić, S. Erhart, and S. Hirche, "Grasp pose estimation in human-robot manipulation tasks using wearable motion sensors", in *2015 IEEE/RSJ International Conference on Intelligent Robots and Systems (IROS)*, IEEE, 2015, pp. 1031–1036.

[29] L. Ljung, "System identification", in *Signal analysis and prediction*, Springer, 1998, pp. 163–173.

[30] S. Hayati, "Hybrid position/force control of multi-arm cooperating robots", in *Proceedings. 1986 IEEE International Conference on Robotics and Automation*, IEEE, vol. 3, 1986, pp. 82–89.

[31] O. Khatib, "Object manipulation in a multi-effector robot system", in *Proceedings of the 4th international symposium on Robotics Research*, MIT Press, 1988, pp. 137–144.

[32] C. Smith, Y. Karayiannidis, L. Nalpantidis, X. Gratal, P. Qi, D. V. Dimarogonas, and D. Kragic, "Dual arm manipulation—a survey", *Robotics and Autonomous systems*, vol. 60, no. 10, pp. 1340–1353, 2012.

[33] S. Erhart and S. Hirche, "Model and analysis of the interaction dynamics in cooperative manipulation tasks", *IEEE Transactions on Robotics*, vol. 32, no. 3, pp. 672–683, 2016.

[34] J. Dumora, F. Geffard, C. Bidard, T. Brouillet, and P. Fraisse, "Experimental study on haptic communication of a human in a shared human-robot collaborative task", in *2012 IEEE/RSJ International Conference on Intelligent Robots and Systems*, IEEE, 2012, pp. 5137–5144.

[35] T. Takubo, H. Arai, Y. Hayashibara, and K. Tanie, "Human-robot cooperative manipulation using a virtual nonholonomic constraint", *The International Journal of Robotics Research*, vol. 21, no. 5-6, pp. 541–553, 2002.

[36] Y. Karayiannidis, C. Smith, and D. Kragic, "Mapping human intentions to robot motions via physical interaction through a jointly-held object", in *The 23rd IEEE International Symposium on Robot and Human Interactive Communication*, IEEE, 2014, pp. 391–397.

[37] T. Wojtara, M. Uchihara, H. Murayama, S. Shimoda, S. Sakai, H. Fujimoto, and H. Kimura, “Human–robot collaboration in precise positioning of a three-dimensional object”, *Automatica*, vol. 45, no. 2, pp. 333–342, 2009.